Steel and Composite Structures, *Vol. 23, No. 1 (2017) 53-66*
DOI: https://doi.org/10.12989/scs.2017.23.1.053

Rotational capacity of pre-damaged I-section steel beams at elevated temperatures

Daphne Pantousa [a] and Euripidis Mistakidis *

Laboratory of Structural Analysis and Design, Department of Civil Engineering, University of Thessaly, Pedion Areos, Volos, Greece

(Received September 12, 2015, Revised November 24, 2016, Accepted December 08, 2016)

Abstract. Structures submitted to Fire-After-Earthquake loading situations, are first experiencing inelastic deformations due to the seismic action and are then submitted to the thermal loading. This means that in the case of steel framed structures, at the starting point of the fire, plastic hinges have already been formed at the ends of the beams. The basic objective of this paper is the evaluation of the rotational capacity of steel I-section beams damaged due to prior earthquake loading, at increased temperatures. The study is conducted numerically and three-dimensional models are used in order to capture accurately the nonlinear behaviour of the steel beams. Different levels of earthquake-induced damage are examined in order to study the effect of the initial state of damage to the temperature-evolution of the rotational capacity. The study starts with the reference case where the beam is undamaged and in the sequel cyclic loading patterns are taken into account, which represent earthquakes loads of increasing magnitude. Additionally, the study extends to the evaluation of the ultimate plastic rotation of the steel beams which corresponds to the point where the rotational capacity of the beam is exhausted. The aforementioned value of rotation can be used as a criterion for the determination of the fire-resistance time of the structure in case of Fire-After-Earthquake situations.

Keywords: rotational capacity; steel beams; fire-after-earthquake; numerical analysis

1. Introduction

In urban areas Fire-After-Earthquake (FAE) is a rather common phenomenon and, occasionally, can be catastrophic. The aftermath of the fire outbreak after an earthquake has many times been witnessed in recent years (Northridge 1994, Kobe 1995, Chile 2010, Tohoku 2011). In many cases, urban environment characteristics (gas piping system, electricity wiring system, etc.) and post-earthquake conditions (multiple ignition points, malfunction of the active fire-protection systems, etc.) are combined and the fire that follows earthquake becomes the predominant cause of damage and loss of human life (Scawthorn *et al.* 2005).

Nowadays, the post-earthquake fire-design is not a normative requirement and the fire design codes assume that when a fire starts, the structure is intact. This is not valid when structures have been damaged due to a prior seismic action. In order to conduct an integrated study for the post-earthquake fire-performance of structures, the seismic damage of structural components needs to be taken into account.

Specifically, considering steel frame structures that are designed according to the ductility requirements of the capacity design rules of EN 1998-1-1 (2004), it is expected that at the starting point of the fire, the plastic hinges have already been (fully or partially) formed at the ends of the beams. On the other hand, the fire design, according to EN 1993-1-2 (2003), of the steel frames is based on the classification of cross-sections, which actually depends on the available rotational capacity of cross-sections at elevated temperatures. In the case of FAE loading, the fire design considerations do not take into account the possible reduction of the rotational capacity of the cross-sections due to the damage that is induced during the seismic excitation. Moreover, during the fire exposure stage, the plastic moment resistance of the cross-section may be further reduced due to the interaction of several phenomena (material degradation, initial imperfections, temperature rise). Therefore, in the case of FAE loading conditions, the classification of the cross-sections during the fire-design may not be realistic since it does not consider the possible reduction of the rotational capacity due to the earthquake induced damage and the reduced plastic moment resistance of the cross-sections at elevated temperatures. The previous indicate that for the FAE loading, the stage of the fire-design should be based on the “modified” rotational capacity and the FAE resistance time should be obtained using criteria that are based on the actual rotational capacity of the structural members.

According to an extended literature survey the unique experimental program concerning the study of the rotational capacity of steel beams at elevated temperatures was conducted by Dharma and Tan (2007a). The main objectives were to determine the effects of temperature on the rotational capacity and to identify the key parameters of the problem. In the companion paper (Dharma and Tan 2007b) numerical models were developed for the prediction of the rotational capacity at elevated temperatures. It is noticed that the aforementioned studies do not consider the

*Corresponding author, Professor
E-mail: emistaki@uth.gr
[a] Dr. Ing., E-mail: dpantousa@gmail.com

http://www.techno-press.org/?journal=scs&subpage=6
ISSN: 1229-9367 (Print), 1598-6233 (Online)

case of pre-damaged beams.

Moreover, concerning the FAE situations, there exist extensive literatures about the disasters that are attributed to the post-earthquake fires in urban regions. Several studies are devoted to the historical events and indicate the mitigation strategies for the reduction of the post-earthquake fire losses in urban regions. On the other hand, the scientific research on the fire-behaviour of unprotected steel structures has only been started. The interest mainly lies on the behavior of steel frame buildings under the FAE loading (Faggiano *et al*. 2007, 2008, Yassin *et al*. 2008, Zaharia *et al*. 2008, 2009, Della Core *et al*. 2003 and Keller 2012, Faggiano and Mazzolani 2011, Keller and Pessiki 2012, Kodur and Dwaikat 2009, Zaharia and Pintea 2009, Lee *et al*. 2008, Zhao 2010). In these studies the criteria used for the determination of the fire-resistance time are based on the strength or stability of structural members or on the global stability of the structure. Effects of the earthquake excitation on the rotational capacity of structural members have not yet been considered.

The present study focuses on the determination of both the rotational capacity and the plastic limit rotations values of a steel I-beam at elevated temperatures, taking into account different levels of initial damage. The damage is induced in the beam using cyclic loading and is expressed in terms of plastic strain. Different levels of damage are considered in order to represent more severe earthquakes. The first goal is to study the available rotational capacity of pre-damaged beams at elevated temperatures and to investigate if the classification that is considered during the fire design of the structural members (according to EN 1993-1-2 (2003)) is applicable also in the case of FAE loading situations. The second goal is the calculation of plastic limit rotation values that can in the sequel be used for the determination of the fire-resistance time of moment-resisting frames under FAE loading. These values could be further used for the design against FAE actions.

2. Definition of rotational capacity

According to the studies of Gioncu and Petcu (2007) and Gioncu and Mazzolani (2002) it is generally accepted that there is no standard definition of the rotational capacity. Three approaches are available: the definition related to the ultimate moment, the definition related to the fully plastic moment and the one related to the post-buckling slope. In this study the definition related to the fully plastic moment is adopted. This definition is given also in the background documentation of Eurocodes. According to this (Fig. 1), the rotational capacity r_α is calculated as

$$r_\alpha = \theta_{ru} / \theta_{pl} \tag{1}$$

or

$$r_{\alpha 0.9} = \theta_{ru0.9} / \theta_{pl} \tag{2}$$

where:

θ_{pl} is the value of rotation that corresponds to the plastic moment resistance of the cross-section, defined as $M_{pl} = f_y w_{pl}$,

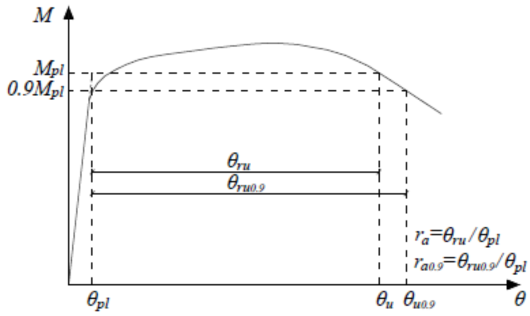

Fig. 1 Definition of the rotational capacity

f_y is the yield stress of steel at room temperature and,

θ_{ru} is the range of the rotation over which the plastic moment resistance of the cross section is retained.

The index 0.9 is used in the case where the rotational capacity is determined using the value of $0.9M_{pl}$. According to Gioncu and Petcu (2007), the selection between the two choices remains a decision of the designer.

It is clarified that in this study the effect of axial forces in the plastic moment resistance of the cross section M_{pl} is not considered. Also, in this study, the index T is added, in order to define the dependence on temperature. Due the fact that at elevated temperatures it is possible that the beam would not able to reach the fully plastic moment M_{plT}, it is more convenient to use the reduced moment for the definition of the rotational capacity, so that it can be calculated in the majority of the cases that are studied. Therefore, the definition of the rotational capacity is based on the value of $0.9M_{pl}$ and the corresponding symbol used is $r_{\alpha 0.9T}$.

3. Description of the problem and assumptions

The main objective of this study is the assessment of the ductility of beams at elevated temperatures in two different cases. In the first case the rotational capacity of the beams is studied under static, monotonic loading at different temperature levels. Regarding the second case, first the beam is subjected to cyclic loading and in the sequel the ductility is obtained for static, monotonic loading at elevated temperatures. The analysis has three different stages. The first stage is the cyclic loading and the other two stages are similar, as in the first case. In fact, in the second case, the cyclic loading induces damage to the beam and the goal is the evaluation of the rotational capacity, depending on the 'level of damage'.

The next objective is to define the limits for the determination of fire-resistance of steel frame structures during fire exposure. These values could be used for the determination of the fire-resistance time of steel framed structures in the case of FAE loading, i.e., when the structure in the start of the fire loading is damaged due to earthquake.

The problem is handled through geometric non-linear finite element analysis taking into account the temperature dependent non-linear material properties. In both cases the numerical model that is developed considers the initial imperfections and parametric analyses are conducted taking into account different amplitudes of the initial geometrical imperfections. In order to simplify the already complex problem, the following assumptions are adopted for the calculation of the moment-rotation curves:

- The temperature is uniform and constant along the beam.
- No-thermal gradient is considered in the cross-section.
- The beam is free to expand longitudinally and, therefore, no thermal compressive forces develop.

4. Validation of the numerical model

Initially, a numerical model is developed for the accurate prediction of the rotational capacity of steel I-beams at elevated temperatures. The model is validated using the test results that are presented in Dharma and Tan (2007a). Briefly, it is referred that the purpose of the experimental study was to define the rotational capacity of a two span continuous steel I-beam under uniform loading, at the possible plastic hinge locations, under fire conditions. Therefore, according to the study, it was important to assess the fire-behaviour of the beam at the hogging moment region, i.e., at the internal supports. In order to simplify the problem, a simply supported beam was considered which was loaded at mid-span.

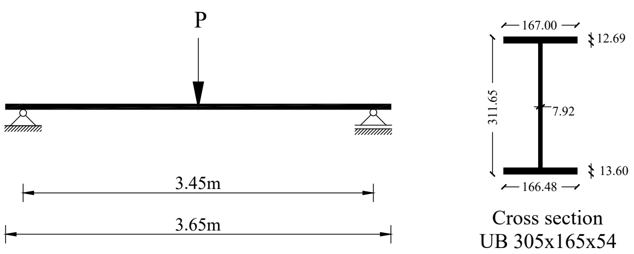

Fig. 2 The structural system and the cross section (dimensions of the cross section in mm)

Table 1 Material properties at ambient conditions

	Yield strength f_{y20}	Ultimate strength f_{u20}	Elastic modulus E_{20}
	(Mpa)	(Mpa)	(Mpa)
Web	307.4	491.4	205253
Flange	297.6	483.6	203677

In this study, for the needs of the validation, the steel I-beam S2-1 is chosen, from the experimental study by Dharma and Tan (2007a). All the geometrical dimensions and the material properties are considered according to this study. In detail, the total length of the simply supported beam is equal to 3.65 m while the distance between the supports is 3.45 m. Also, web stiffeners are used at the support and at mid-span, where the load is applied. The beam is laterally restrained at the position of supports at both ends and at mid-span. Therefore, the effective length of the beam for lateral torsional buckling is equal to 1.725 m. The cross-section dimensions and the structural system are illustrated in Fig. 2. The material properties at room temperature are defined from tensile tests and they are presented in Table 1.

It is stressed that the beam is laterally restrained only at the ends and at mid-span and, therefore, the development of plastic lateral-torsional buckling is possible under certain conditions at elevated temperatures. Moreover, plastic local buckling may arise.

4.1 The numerical model used for the validation

The numerical model is developed using the nonlinear finite element code MSC-MARC (2010). The three-dimensional numerical model (Fig. 3) utilizes four-node, thick-shell elements. The numerical model takes into account the nonlinear elastic-plastic stress-strain relationship of steel at elevated temperatures. The yield stress, the proportionality limit and the elastic modulus are temperature dependent following the temperature relationships given in EN 1993-1-2 (2003).

Concerning material modelling, the Von Mises yield criterion is used in the numerical analysis. Additionally, the analysis takes into account the geometric non-linearity.

Concerning the material modelling, the actual material properties for the specific steel used in the experiment were followed and the values of the tensile coupon tests were adopted for both the web and the flange. Moreover, following experimental observations that indicate that steel keeps a significant hardening even in the case of 400°C (Poh 2001, Kodur and Dwaikat 2009), the hardening of steel was taken into account for temperature equal to 400°C. More specifically, the ultimate strength was taken as $f_{u,T} = 1.6 f_{y,T}$ for temperature range between 20°C and 400°C.

Initial imperfections are incorporated in the geometry of the steel beam for a more realistic assessment of its behaviour. There are many different ways to introduce initial geometric imperfections in structural members. A simple way in the context of finite element analysis is to

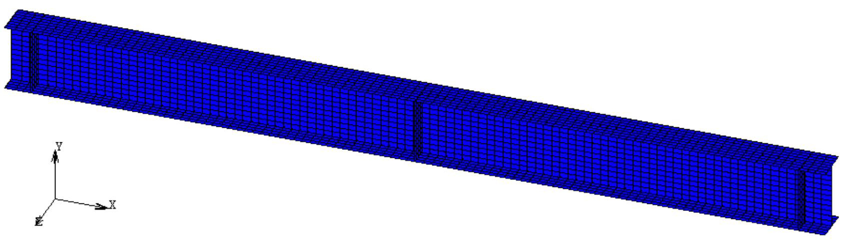

Fig. 3 The numerical model

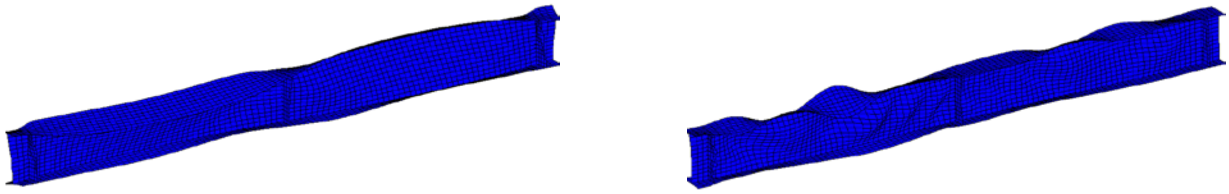

(a) Eigenmode corresponding to the lateral torsional buckling (b) Eigenmode corresponding to the local buckling of the upper flange

Fig. 4 Results of the buckling analysis

extract the buckling eigenmodes and introduce them as imperfections with specific amplitude. More specifically, the normalized buckling mode is multiplied by a scale factor, leading to certain maximum amplitude and the resulting displacements are added to the initial coordinates of the structural member. For the case studied here, two different eigenmodes are combined (see details in Fig. 4). The first eigenmode is related with the local buckling along the upper flange of the beam (where compressive stresses arise under the considered loading) while the second buckling eigenmode used is the one corresponding to the development of lateral torsional buckling.

The amplitude of the initial imperfections used for the analysis is taken equal to 0.5 mm for the buckling eigenmode which is related to the lateral torsional buckling and to 2 mm for the eigenmode which is related to the local buckling of the upper flange. These values are in accordance with the maximum values of the measured initial imperfections that are presented in Dharma and Tan (2007a).

The numerical analysis has two different stages, following the test procedure described in Dharma and Tan (2007a). At the first stage the steel beam is heated with a heating rate equal to 7°C/min until the desired temperature T is reached. It must be noticed that during the heating stage the temperature is supposed to be uniform along the member. At the second stage the temperature remains constant and the beam is submitted to loading at mid-span until failure.

4.2 Comparison with the test results

The primary objective in this section is to validate the numerical model against the published experimental results presented in the study of Dharma and Tan (2007a).

Fig. 5 illustrates the load-displacement curves obtained numerically and experimentally for the modelled specimen S2-1. A very good agreement is obtained for the initial stiffness and for the maximum load of the system. Moreover, the softening branch is well approximated by the numerical model. A small difference is observed for the maximum strength of the steel beam that can be attributed to the lack of actual experimental data for the ultimate and the yield strength of steel at elevated temperatures. Also, the small differences between the numerical and the test results at the unloading branch may attribute to the uncertainties connected to the profile of the initial imperfections. Additionally, the failure mode that results from the numerical analysis is very close to the experimentally obtained one, as it is presented in Fig. 6. In both cases the failure is due to lateral – torsional buckling of the steel beam.

Taking into account the previous, it is considered that the developed numerical model is able to accurately simulate the behaviour of the steel I-beam at elevated temperatures. Additionally, it is indicated that the shapes of the initial imperfections that were adopted can be used for the purpose of parametric studies.

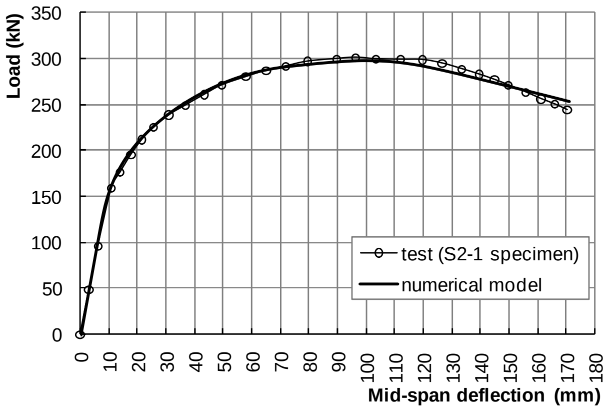

Fig. 5 Comparison of the numerical analysis results with the test results for the specimen S2-1 at 415°C

(a) Test results

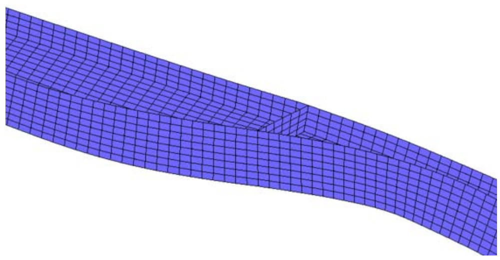

(b) Numerical analysis results

Fig. 6 Deformed shape of the steel beam at the failure

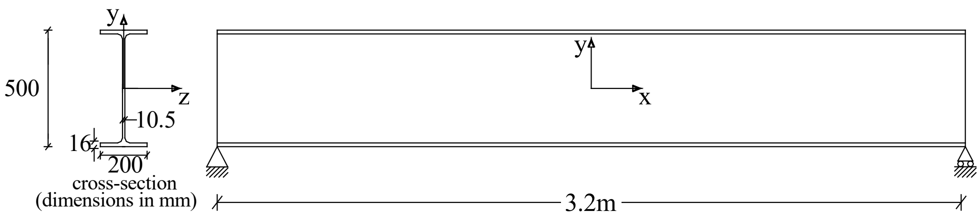

Fig. 7 Geometry of the considered steel beam

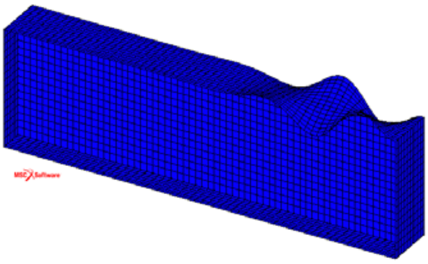

(a) The upper flange eigenmode

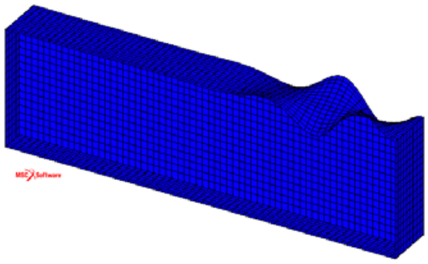

(b) The lower flange eigenmode

Fig. 8 Results of the buckling analysis

5. The numerical model used for the determination of the rotational capacity

The model validated in the previous paragraph against experimental results, is now used for the evaluation of the ductility of the structural members. Specifically, three different issues are addressed. The calculation of the moment-rotation curves, the evaluation of the rotational capacity and the determination of the limit values of rotation at elevated temperatures. In order to simulate FAE loading situations the study is extended to include cyclic loading, introducing a certain level of damage in the steel beam prior to the temperature increase.

For this reason the numerical model is adjusted in order to take into account the behaviour of steel beams under cyclic loading. The supplementary assumptions adopted in the analyses that were performed are the following:

- The beam is sufficiently laterally restrained and lateral-torsional buckling cannot occur. Subsequently, the initial imperfections that are used are related only to the local buckling failure modes and not to the global one. This assumption is adopted in order to conduct a more rational study that can be used for practice design purposes. Moreover, it is compatible with the actual situation in buildings, where the lateral torsional buckling is usually restrained by the presence of a concrete slab.
- The initial imperfections concerning the local buckling of the flanges are symmetric. This assumption is adopted due to the fact that the results of the buckling eigenmode analysis indicate that the first local buckling mode is symmetric. As it is expected, the outcomes of the analysis are not the same with those that would result in the case where asymmetric eigenmodes are employed.
- The strain hardening branch of the stress-strain law of steel (for the temperature range between 20°C-400°C) is not taken into account and the isotropic hardening rule is used.

5.1 Geometry and initial imperfections

The geometric characteristics of the numerical model used for the determination of the rotational capacity, are described in Fig. 7. The span of the beam, considered as an example, is 3.2 m.

In order to reduce the computational cost associated with the nonlinear three-dimensional modeling, only half of the total length of the beam is considered, using the appropriate symmetry boundary conditions. The initial imperfections that are incorporated in the geometry of the steel beam are depicted in Fig. 8. Specifically, two different eigenmodes are combined. The first eigenmode is related to the first local buckling mode at the upper flange of the beam, which is anti-symmetric with respect to the *x-y* plane, while the second eigenmode used is the corresponding mode for the lower flange of the beam. The study includes the imperfections of both flanges, in order to obtain more realistic results in the case of the FAE loading, since the compressive zone shifts during the cyclic loading.

6. Simulation of three point bending tests at elevated temperatures

In order to determine the rotational capacity, virtual three point bending tests are performed according to Dharma and Tan (2007a). First, the reference case where the beams are not damaged due to seismic excitation is studied. The numerical analysis conducted for the simulation of these tests follows two different stages. In the first stage the temperature increases until the desired level is attained. During this stage the beam is not mechanically loaded, as depicted in Fig. 9. The mechanical loading stage follows (three-point bending), while the temperature remains

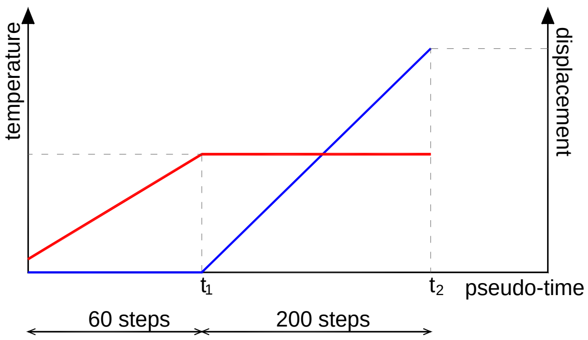

Fig. 9 Case 1: loading procedure

constant. It is noted that the numerical test is displacement controlled.

The test is repeated for nine temperature levels between 20°C and 800°C. Parametric analyses are conducted with respect to the amplitude of initial imperfections. Specifically, three different cases are studied for amplitudes equal to 0.5 mm, 2 mm and 5 mm respectively. Also, the case where the model does not include initial imperfections (perfect model) is studied for reference. It is clarified that in this study the term "perfect model" is used to denote the model that does not include geometrical imperfections.

6.1 The moment-rotation curves

The moment-rotation curves obtained for the various temperature levels are presented in Fig. 10. Imperfections sensitivity study is conducted in order to quantify their effect on the ultimate capacity and furthermore to the rotational capacity of the beam. Table 2 presents the moment resistance considering both the results from the FEM analyses and the corresponding values according to the calculations based on the plastic resistance of the cross-section. Moreover, Table 2 presents the comparison of the ultimate moment resistance that is obtained from the analyses using the perfect models with the corresponding values when initial imperfections are used. The comparison indicates that the incorporation of the initial imperfections of the beam geometry results to the reduction of the ultimate load bearing capacity of the beam and this is more obvious at elevated temperatures. The reduction presented in Table 2 is calculated with respect to the moment resistance that results from the FEM analysis where the model is considered to be perfect. The results indicate that the reduction becomes important as the temperature and the amplitude of the initial imperfections increase.

Furthermore, it can be observed that the rotation that corresponds to the ultimate moment capacity of the beam (Table 2) is increased as the temperature rises. This can be attributed to the elliptic plastic branch that is incorporated in the stress-strain relationship of steel at elevated temperatures, according to Fig. 3 of EN-1993-1-2 (2003). This branch connects the elastic and the perfectly plastic ones and causes the increased values of strain that correspond to the yield stress compared to the respective value at room temperature. On the other hand, as the amplitude of initial imperfections increases, the rotation that corresponds to the ultimate moment capacity is considerably reduced, as it is indicated in Table 2.

Additionally, it is interesting to notice the effect of the amplitude of the initial imperfections on the descending

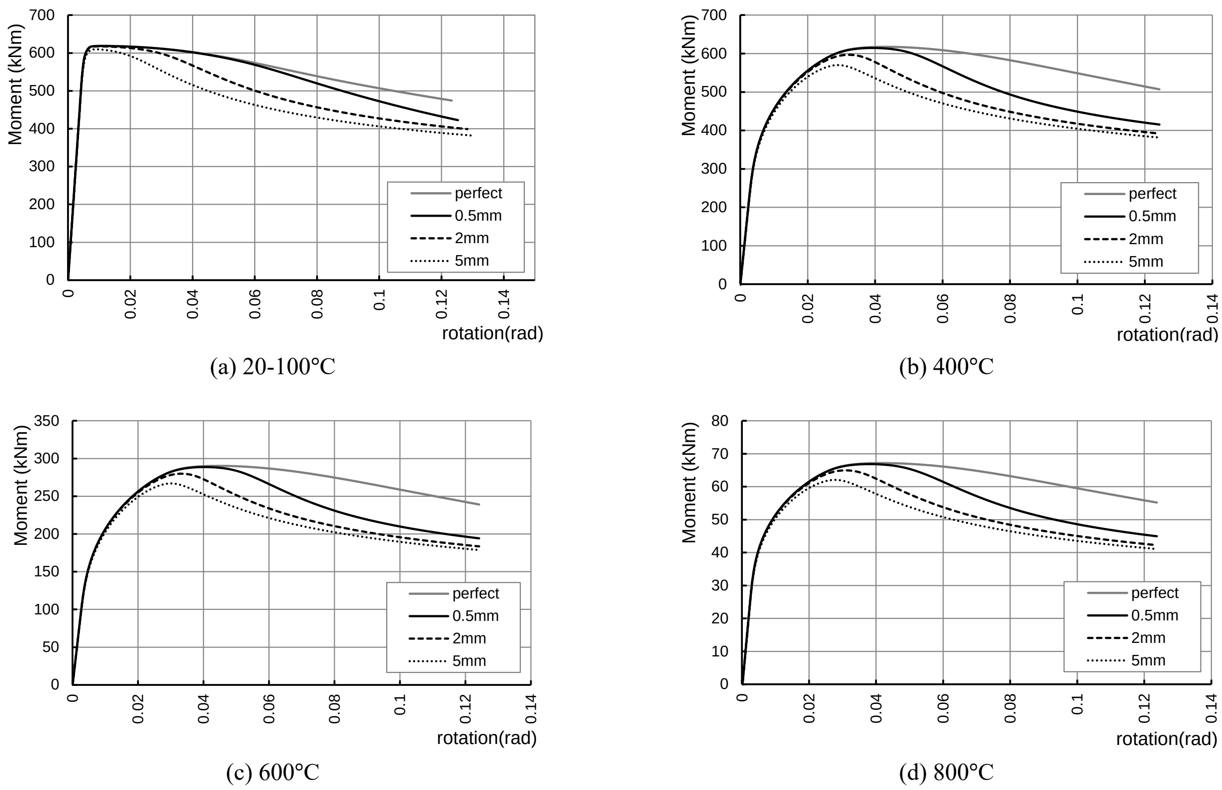

Fig. 10 Moment-rotation curves at different temperature levels and for various amplitudes of initial imperfections

Table 2 The moment resistance of the beam and the maximum rotation at different temperature levels

T (°C)	20/100	200	300	400	500	600	700	800
M_{pl} (KNm)[1]	603.35	603.35	603.35	603.35	470.61	283.57	138.77	66.37
Perfect model								
M_u (KNm)[2]	618.67	616.33	616.86	617.47	481.99	290.24	141.55	67.17
θ_{max} (rad)[4]	0.011	0.027	0.036	0.043	0.041	0.045	0.047	0.042
Amplitude of initial imperfections 0.5mm								
M_u (KNm)[2]	618.62	615.38	614.89	614.58	479.96	288.71	140.62	66.87
Moment reduction[3]	0.01%	0.15%	0.32%	0.47%	0.42%	0.53%	0.66%	0.45%
θ_{max}[4]	0.011	0.026	0.033	0.039	0.038	0.040	0.042	0.038
θ_{max} reduction[5]	0.00%	4.52%	8.53%	9.87%	8.87%	9.56%	10.29%	8.74%
Amplitude of initial imperfections 2mm								
M_u (KNm)[2]	617.56	606.09	600.26	596.75	466.70	279.86	135.88	64.97
Moment reduction[3]	0.18%	1.66%	2.69%	3.36%	3.17%	3.58%	4.01%	3.28%
θ_{max} (rad)[4]	0.010	0.020	0.027	0.032	0.031	0.033	0.035	0.031
θ_{max} reduction[5]	5.51%	24.97%	25.78%	25.58%	25.35%	24.80%	25.99%	26.46%
Amplitude of initial imperfections 5mm								
M_u (KNm)[2]	609.89	587.11	576.34	570.03	446.39	266.95	129.28	62.08
Moment reduction[3]	1.42%	4.74%	6.57%	7.68%	7.39%	8.02%	8.67%	7.58%
θ_{max} (rad)[4]	0.009	0.018	0.023	0.029	0.028	0.030	0.032	0.028
θ_{max} reduction[5]	16.34%	34.15%	34.58%	32.89%	33.02%	31.89%	32.71%	34.03%

[1] According to the elastic-plastic cross-section analysis
[2] According to FEM results
[3] Reduction with respect to the moment resistance that results from the FEM analysis where the model is considered to be perfect
[4] Rotation that corresponds to the ultimate moment capacity
[5] Reduction with respect to the maximum rotation that results from the FEM analysis where the model is considered to be perfect

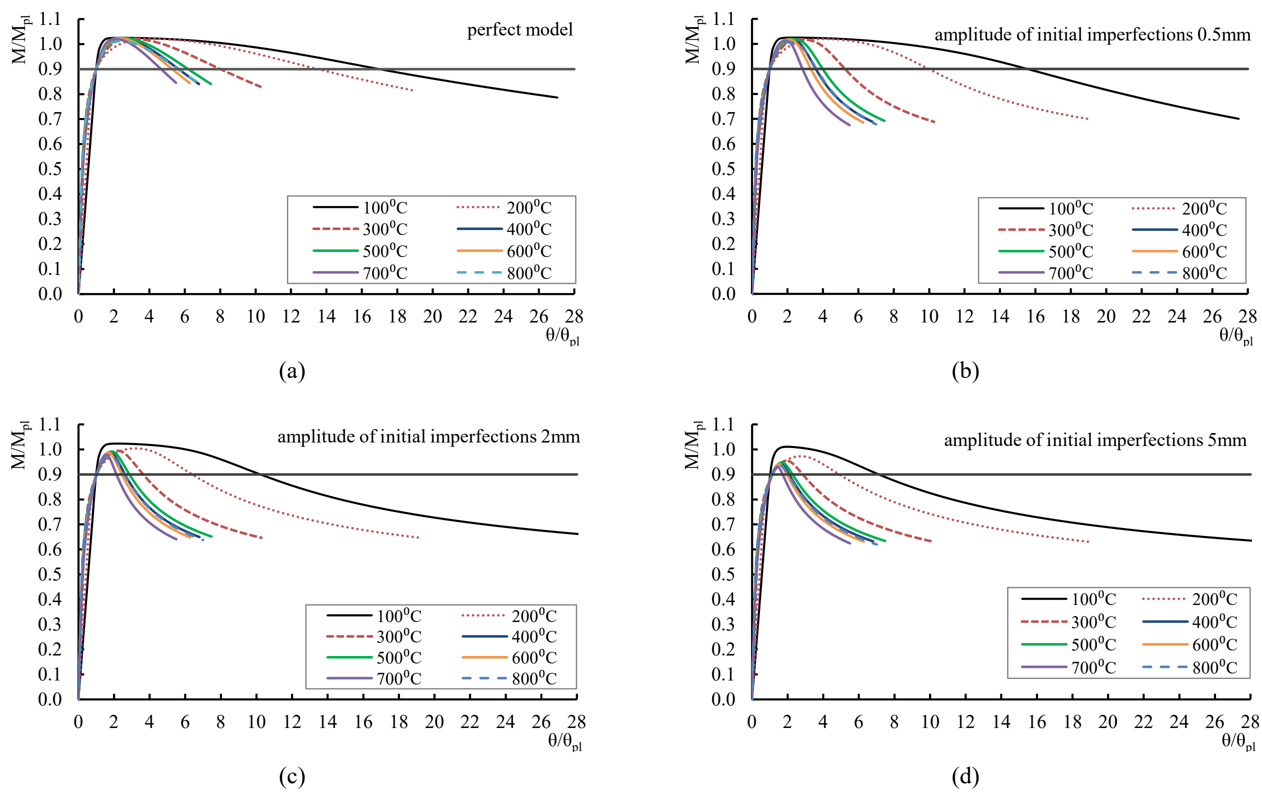

Fig. 11 Effect of the temperature on the moment-rotation diagrams for different amplitudes of initial imperfections

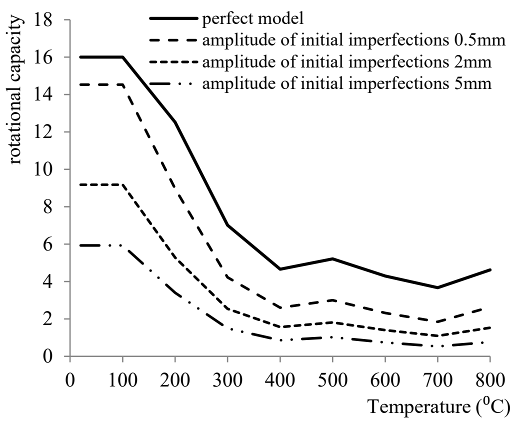

Fig. 12 The evolution of the rotational capacity with the temperature and the effect of the amplitude of the initial imperfections

branch of the curve. The diagrams show that as the magnitude of the initial imperfection increases, the descending branch becomes steeper. This holds for all the imperfect models at both room conditions and at elevated temperatures.

6.2 The dimensionless moment-rotation curves and the rotational capacity

In order to compare the results in different temperature levels in a more systematic way and to calculate the rotational capacity, it is necessary to use dimensionless values for the moment and the rotation. The dimensionless moment-rotation curves are presented in Fig. 11. Concerning the moment, M_{plT} is used for the normalization, which is the plastic moment resistance defined as $M_{plT} = f_{yT}w_{pl}$. For the rotation, the normalization is based on θ_{plT}. This value is taken according to the results of the corresponding analyses (Table 2).

Next, the rotational capacity $r_{0.9T}$ is evaluated using the dimensionless curves. As it was previously referred, the rotational capacity is obtained using the value $0.9M_{plT}$. In Fig. 12 it is clearer that the rotational capacity is reduced as the temperature increases and this holds for both the "perfect" and the "imperfect" models. It is noted that the rotational capacity is slightly increased at 500°C and 800°C. This can be connected to the ratio of the modulus of elasticity to the yield stress at elevated temperatures. Specifically, if the evolution of this ratio with temperature is plotted, the same phenomenon is also present (Fig. 5, Franssen and Vila Real 2010). Moreover, it is noticed that the amplitude of the initial imperfections has a dominant effect to the rotational capacity and, specifically, as the amplitude increases, the rotational capacity is considerably reduced.

7. Virtual three point bending tests of beams pre-damaged due to cyclic loading, at elevated temperatures

In the previous section the reference case where the beams are considered undamaged is presented. In order to study in a more realistic manner the performance of structural members under FAE loading, the earthquake induced damage should be considered. It is essential to include this damage in order to quantify the effect of seismic excitation to both the rotational capacity and the ultimate moment resistance of cross-sections.

Considering the previous, in this study the cyclic loading is introduced in order to induce a certain level of damage in the beam. Specifically, this simulates the damage that is induced in the beams of a frame structure, due to earthquake loading. The level of damage induced in the frame structure varies and depends on the accelerogram that is used and on the scale factor that is considered. Taking into account the previous, it is obvious that different patterns of cyclic loading should be used in order to simulate different levels of damage induced in the beam.

The numerical analysis that is conducted for the simulation of three point bending test of pre-damaged beams has three different stages. The analysis is displacement controlled. The first stage is the cyclic loading which induces a certain level of plastic deformations (damage) in the beam. In the second stage the temperature increases until the desired level is reached. The monotonic loading stage follows, while the temperature remains constant.

The determination of the pattern of the cyclic loading is crucial since the point where this stage ends defines the initial configuration of the beam for the next stage. Actually, three different possibilities can be considered for the point where the cyclic loading is terminated. The behaviour of the beam is depicted through the total reaction force-displacement curves (total reaction force includes both reactions of the beam). The first one (configuration a) corresponds to the state where the imposed displacement becomes zero but the reaction is not eliminated. In the second case (configuration b) the beam does not return to the initial position, thus the displacement is not equal to zero but the reaction is eliminated. In the third case (configuration c), at the end of the cyclic loading both the displacement and the reaction are zero (Fig. 13).

The behaviour of the beam during the thermal loading stage depends on the configuration of the beam at the beginning of the stage. In the case where residual forces are present in the beginning of thermal loading (configuration a) the beam deflects under these forces when the temperature rises and this is not expected to happen. This can be avoided using configurations b or c. In the case of configuration b, residual displacements remain at the end of the cyclic loading, something that makes the subsequent results dependent on the direction of the monotonic loading. In order to overcome the above problems, configuration c is finally adopted. The three different stages are illustrated in Fig. 14.

7.1 The considered cyclic loading patterns

Five different cyclic loading patterns are studied and they are presented in Fig. 15. The cyclic loading (displacement controlled) is conducted actually for one and a half cycle. During the first cycle, the amplitude of the imposed

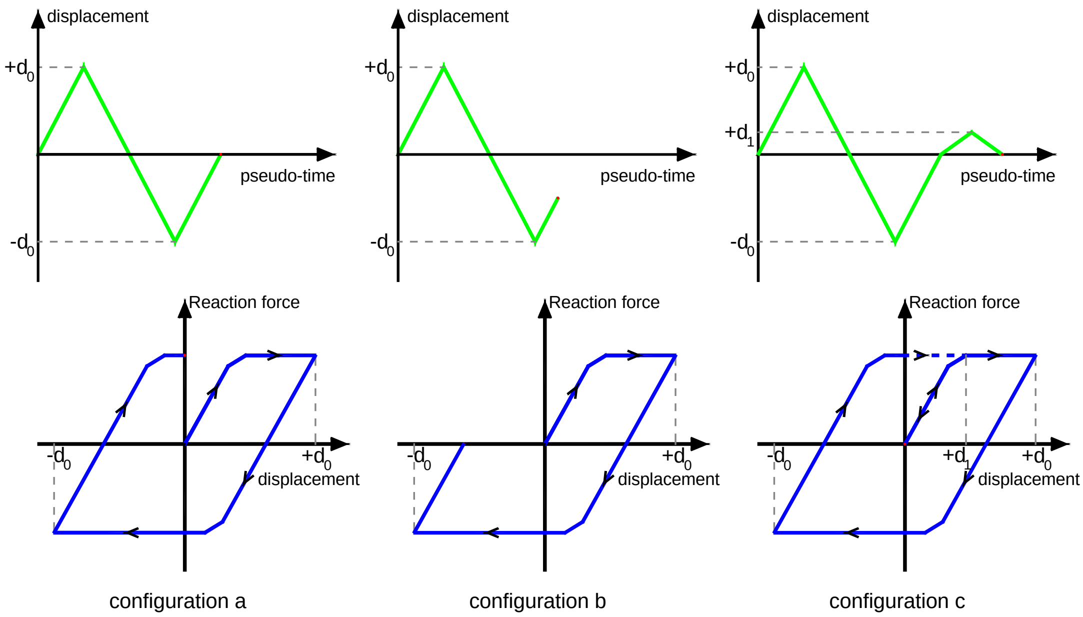

Fig. 13 Different configurations concerning the cyclic loading

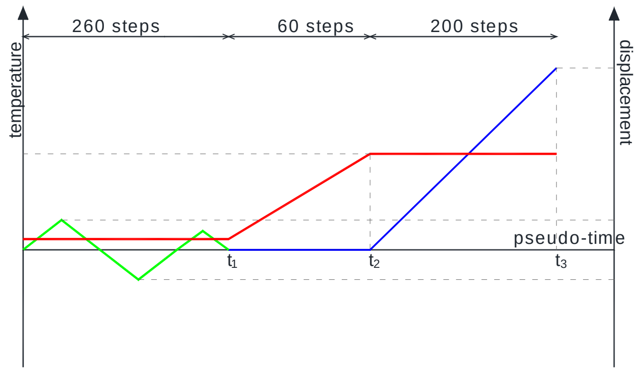

Fig. 14 Case 2: loading procedure

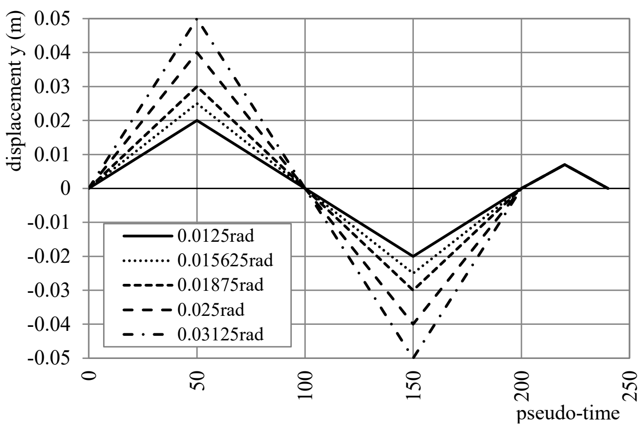

Fig. 15 Cyclic loading patterns

displacement varies between 0.02 m and 0.05 m for the different patterns that are considered, as it is illustrated in Fig. 15. Specifically, first the maximum value of the displacement is reached, then it is reduced until the negative maximum (same) value is attained and in the following the imposed displacement is eliminated. The final half pattern that follows is the same for all the considered cases and aims to the attainment of the configuration where both the displacement and the reaction are zero. The designation of the patterns is based on the magnitude of the imposed rotation on the beam, as it can be observed in Fig. 15.

The "level of damage" induced in the beam during the cyclic loading stage depends on the amplitude of the imposed displacement. This can be clear if the plastic deformation field is considered. Thus, the results of the analyses that follow are dependent on the cyclic loading pattern that is used.

7.2 Moment-rotation curves for the monotonic loading

Figs. 16 and 17 depict the moment-rotation curves corresponding to the monotonic loading stage (3rd stage of the loading procedure of Fig. 14). The comparison is carried-out with respect to the 'level of damage' induced during the cyclic loading stage for every temperature level and for different amplitudes of initial imperfections. It is noted that the ultimate moment resistance of the beam is slightly reduced as the 'level of damage' increases. This holds for small amplitudes of initial imperfections. As the amplitude increases, the reduction becomes significant. Table 3 presents the ultimate moment resistance of the pre-damaged beam at different temperature levels. It is observed that the reduction of the moment resistance with respect to the calculated plastic resistance of the cross-section is independent of the temperature level and is almost equal to 1%, 5% and 10% for amplitude of initial imperfections 0.5 mm, 2 mm and 5 mm respectively. The previous values correspond to the maximum reduction that is obtained and it is referred to the case where the imposed rotation during the cyclic loading is 31.25 mrad.

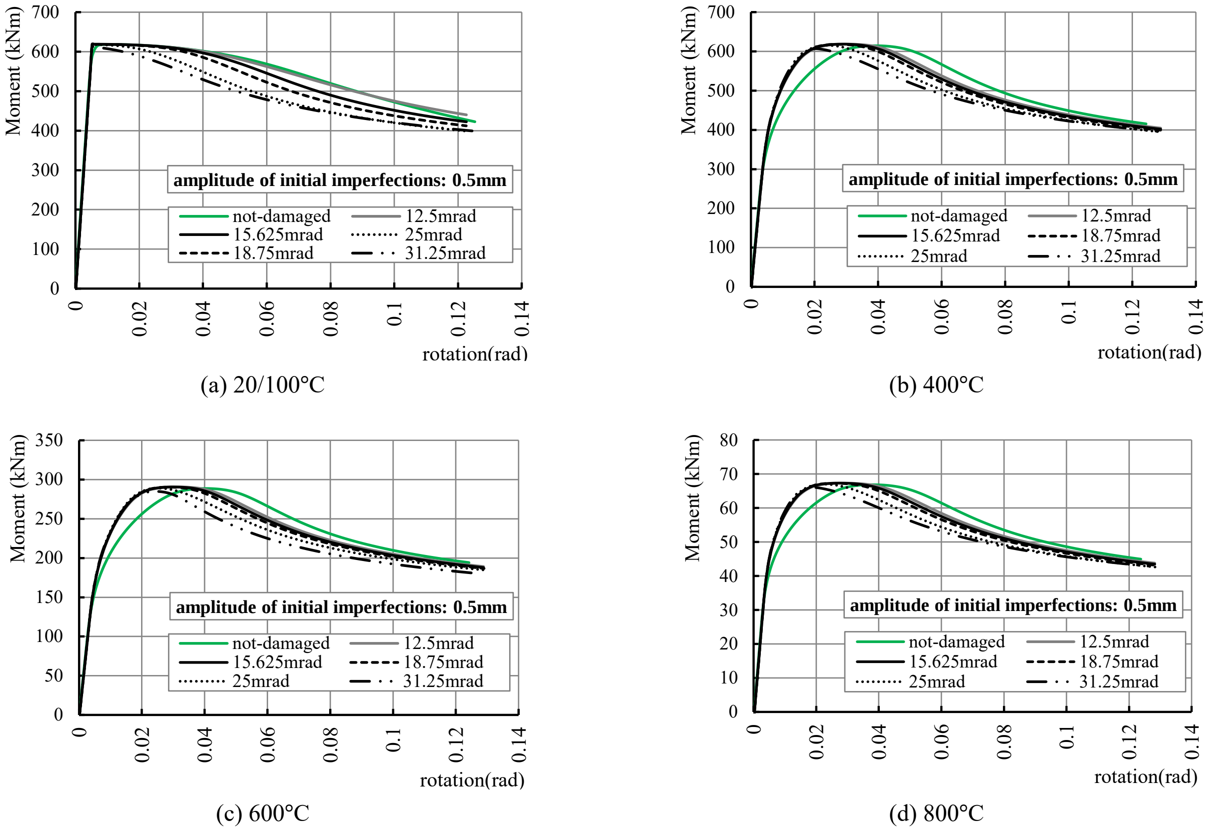

Fig. 16 Moment-rotation curves for the monotonic loading stage of three-point bending test concerning pre-damaged beams (amplitude of initial imperfections equal to 0.5 mm)

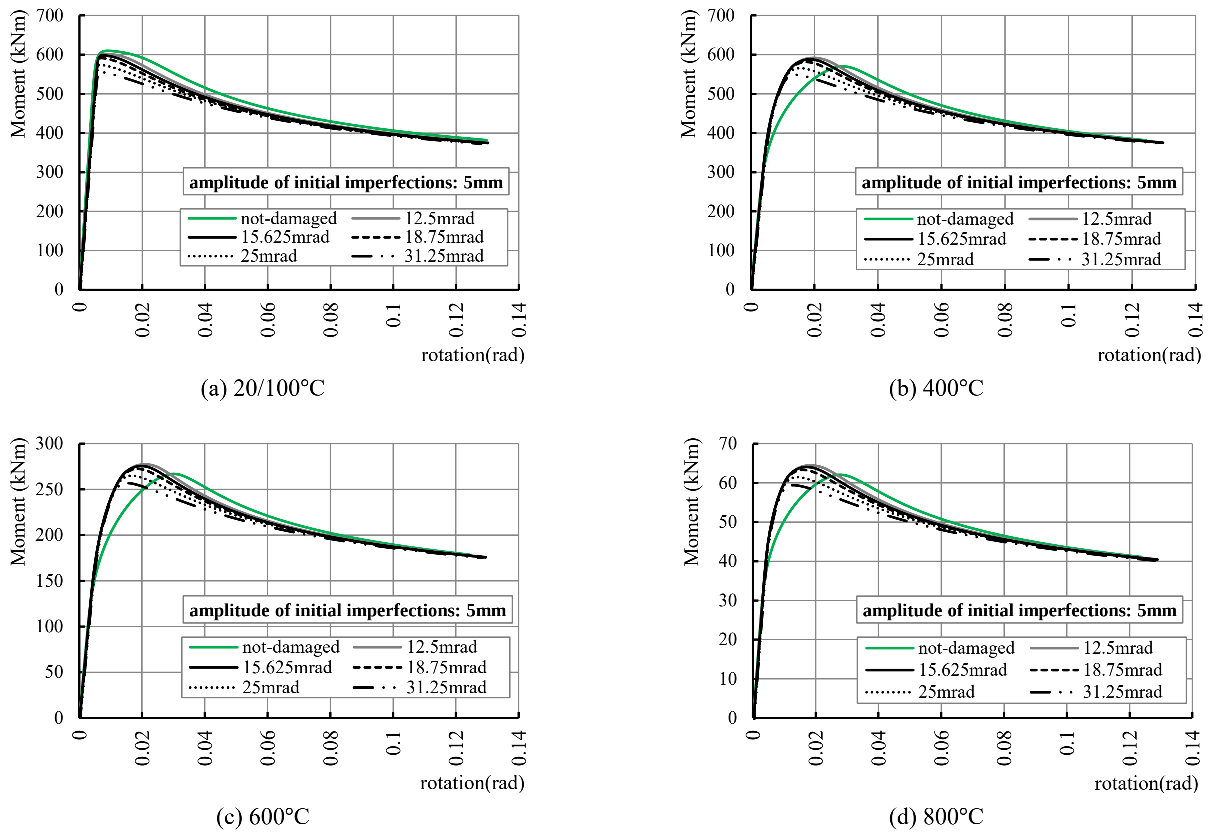

Fig. 17 Moment-rotation curves for the monotonic loading stage of three-point bending test concerning pre-damaged beams (amplitude of initial imperfections equal to 5 mm

Table 3 The moment resistance of the beam and the maximum rotation at different temperature levels considering the amplitude of initial imperfections

T (°C)		20/100	200	300	400	500	600	700	800
Moment resistance (KNm)		618.62	615.38	614.89	614.58	479.96	288.71	140.62	66.87
Amplitude of initial imperfections 0.5 mm									
12.5 mrad	M_u (KNm)	618.90	618.38	618.56	618.72	483.13	290.72	141.64	67.34
	θ_{max} (rad)	0.008	0.017	0.024	0.030	0.028	0.031	0.033	0.029
15.625 mrad	M_u (KNm)	618.94	618.37	618.44	618.58	483.05	290.64	141.60	67.33
	θ_{max} (rad)	0.006	0.016	0.022	0.029	0.027	0.030	0.032	0.027
18.7 mrrad	M_u (KNm)	618.89	618.19	618.09	618.16	482.73	290.43	141.48	67.28
	θ_{max} (rad)	0.006	0.014	0.021	0.028	0.025	0.028	0.030	0.026
25 mrad	M_u (KNm)	618.17	616.79	615.93	615.62	480.88	289.16	140.76	67.02
	θ_{max} (rad)	0.005	0.010	0.018	0.024	0.022	0.025	0.028	0.022
31.25 mrad	M_u (KNm)	612.12	610.48	608.34	607.09	474.48	285.02	138.55	66.10
	θ_{max} (rad)	0.005	0.008	0.014	0.021	0.018	0.024	0.024	0.018
Moment reduction (%)[1]		1.05	1.05	0.80	1.06	1.22	1.14	1.28	1.47
Amplitude of initial imperfections 2 mm									
12.5 mrad	M_u (KNm)	617.04	613.28	609.78	607.39	474.89	285.02	138.51	66.16
	θ_{max} (rad)	0.006	0.011	0.017	0.023	0.022	0.024	0.027	0.022
15.625 mrad	M_u (KNm)	616.19	612.55	608.73	606.27	474.03	284.48	138.22	66.04
	θ_{max} (rad)	0.005	0.010	0.016	0.022	0.020	0.023	0.025	0.020
18.7 mrrad	M_u (KNm)	614.33	610.99	606.90	604.20	472.50	283.48	137.65	65.82
	θ_{max} (rad)	0.005	0.009	0.015	0.021	0.019	0.022	0.024	0.019
25 mrad	M_u (KNm)	605.07	603.47	599.62	596.47	466.59	279.75	135.74	64.97
	θ_{max} (rad)	0.005	0.007	0.013	0.019	0.017	0.020	0.022	0.017
31.25 mrad	M_u (KNm)	590.54	590.12	587.72	584.88	457.43	277.46	133.04	63.61
	θ_{max} (rad)	0.006	0.007	0.012	0.017	0.016	0.021	0.021	0.016
Moment reduction (%)[1]		4.54	4.10	4.42	4.83	4.69	3.90	5.39	4.87
Amplitude of initial imperfections 5 mm									
12.5 mrad	M_u (KNm)	605.79	601.78	596.18	591.83	463.13	277.46	134.59	64.49
	θ_{max} (rad)	0.006	0.009	0.014	0.020	0.018	0.021	0.023	0.018
15.625 mrad	M_u (KNm)	600.97	598.04	592.49	587.95	460.17	275.60	133.64	64.06
	θ_{max} (rad)	0.005	0.007	0.013	0.019	0.017	0.020	0.022	0.017
18.7 mrrad	M_u (KNm)	593.37	591.25	586.15	581.39	455.10	272.48	132.04	63.32
	θ_{max} (rad)	0.005	0.007	0.012	0.017	0.016	0.019	0.021	0.016
25 mrad	M_u (KNm)	593.37	574.05	570.30	565.58	442.83	264.99	128.31	61.47
	θ_{max} (rad)	0.005	0.007	0.010	0.015	0.014	0.017	0.019	0.015
31.25 mrad	M_u (KNm)	557.31	556.25	553.11	548.66	429.65	256.98	124.30	59.41
	θ_{max} (rad)	0.005	0.007	0.009	0.014	0.012	0.015	0.017	0.013
Moment reduction (%)[1]		9.91	9.91	9.61	10.05	10.73	10.48	10.99	11.61

[1] The reduction is calculated with respect to the plastic moment resistance of the cross-section

Additionally, it can be noticed that the rotation that corresponds to the ultimate moment resistance is reduced as the 'level of damage' induced during the cyclic loading is increased. This is valid for all the amplitudes of the initial imperfections that are considered.

7.3 Rotational capacity

The evolution of the available rotational capacity of the beam with temperature is depicted in Fig. 18 considering the amplitude of the initial imperfections and the magnitude of the imposed rotation during the cyclic loading. It is obvious that the rotational capacity is reduced at elevated temperatures. Moreover, as the 'level of damage' increases, the capacity of the beam reduces and this becomes more

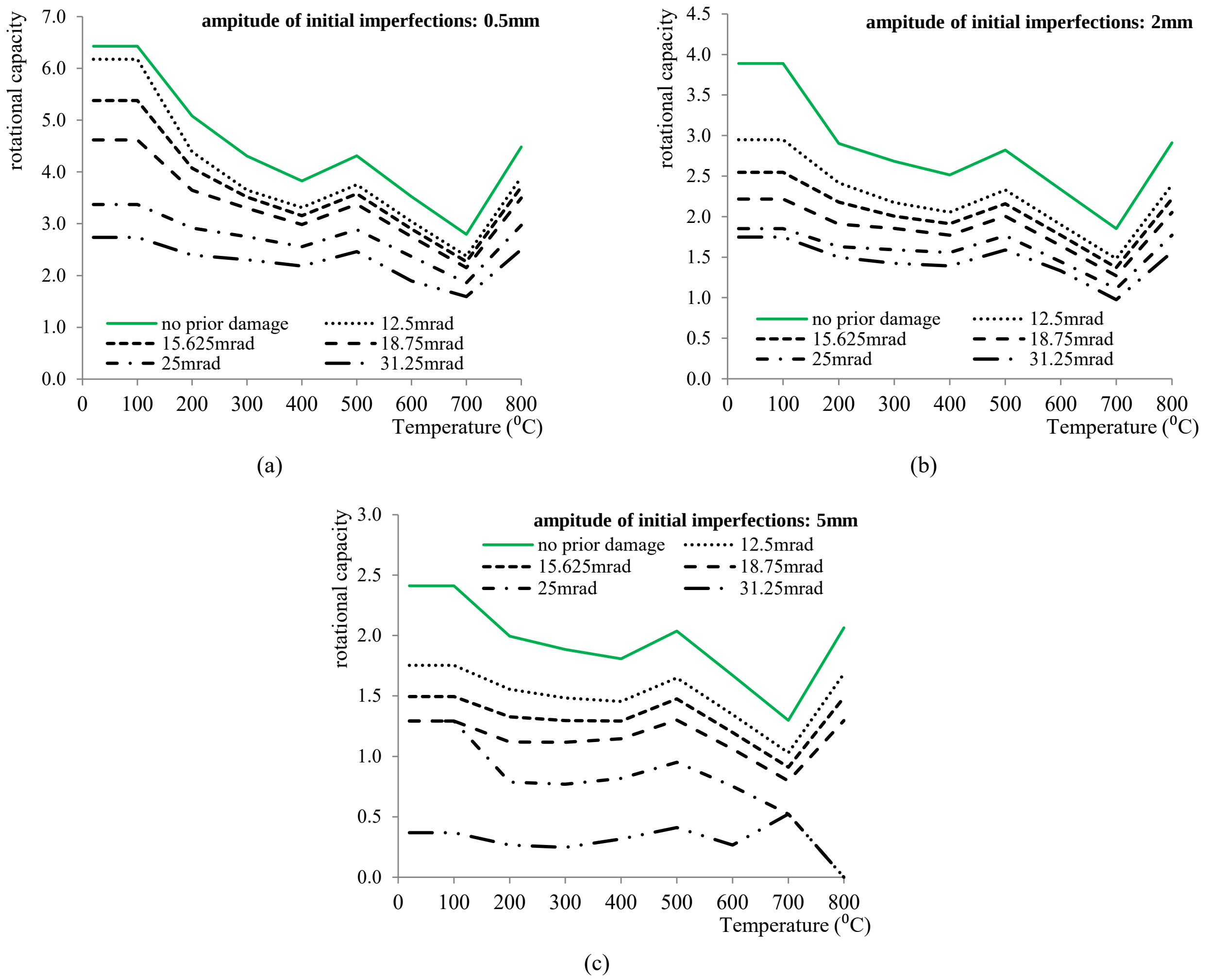

Fig. 18 Available rotational capacity of the pre-damaged beams for different levels of damage considering the effect of the initial imperfections

critical as the amplitude of the imperfections is enlarged. It is noted that at 700°C and 800°C, for amplitude of the initial imperfections 5mm and in the case where the magnitude of the imposed rotation during the cyclic loading is equal to 25 mrad and 31.25 mrad, the moment resistance of the beam does not exceed the value $0.9M_{pl,T}$. This indicates that the rotational capacity of the beam becomes zero.

It can be concluded that the classification of the specific cross-section (Class 1 at elevated temperatures for bending about the major axis) does not hold in the case of FAE loading. It can be noticed that if the earthquake-induced damage is considered, the cross-section can develop the plastic-moment resistance at elevated temperatures, but the rotation capacity is limited due to the development of local buckling. This indicates that the classification of the cross-section results to Class 2. In the limit case where the amplitude of initial imperfections is considered to be equal to 5 mm, Class 3 should be taken into account.

7.4 Proposal for failure criterion in case of FAE

The fire-resistance time of steel frame structures under FAE loading can be determined either using strength or stability criteria. In this section the proposed criterion is based on the ultimate value of the rotation (θ_{ru}) of beams (termed in the sequel as "ultimate available rotation") since it is ensured that the global buckling is prevented. The advantage of using this criterion is that the earthquake-induced damage can also be considered. Moreover, the proposed criterion takes into account the existence of initial imperfections and the possible local buckling phenomena that may arise. Since the value of the ultimate rotation corresponds to the exhaustion of the rotational capacity of the cross-section, this value is actually a limit value and the structural member cannot carry furthermore the applied loading. In this point of view, the ultimate value of rotation can be proposed as a criterion for the identification of the failure of the structure during the fire i.e., for the determination of the fire-resistance time. The ultimate values of rotation could be utilized during the FAE design, using appropriate safety factors in a manner similar to the performance-based design procedure that is used in earthquake engineering.

The change of the values of ultimate available rotation with temperature are presented in Fig. 19. It is noticed that as the temperature rises, the ultimate available rotation is at first reduced and in the sequel it is slightly increased. On

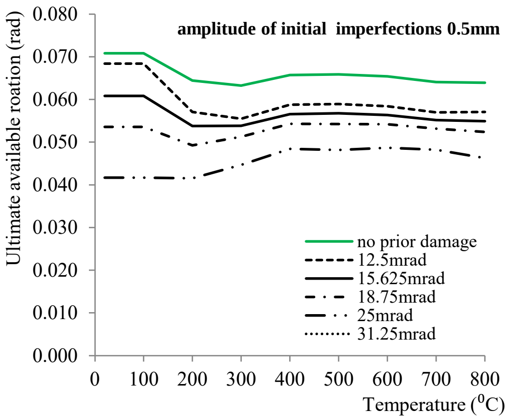

(a)

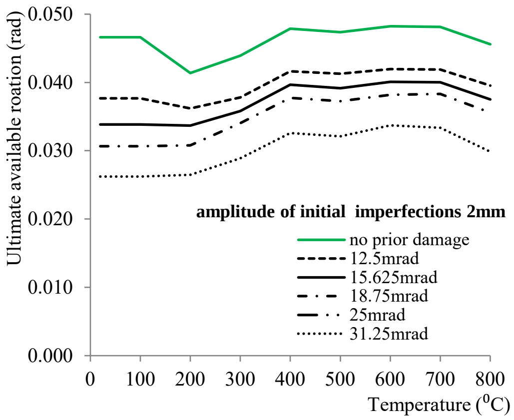

(b)

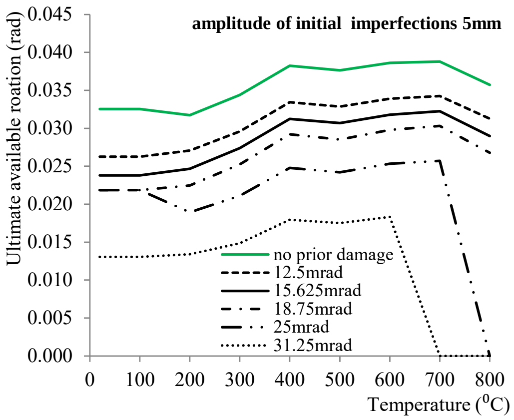

(c)

Fig. 19 Ultimate available rotation of the pre-damaged beams for different levels of damage considering the effect of the initial imperfections

the other hand, the "level of damage" induced due to cyclic loading affects strongly the ultimate available rotation. Specifically, the aforementioned rotation is considerably reduced when the "level of damage" is enlarged and this becomes more important as the amplitude of the initial imperfections increases.

It has to be stressed that the present paper aims to designate an alternative failure criterion for the design of steel beams in case of FAE situations, rather than to propose actual values for the general case. These values should be determined after the elaboration of a number of both real and virtual tests that will examine in detail all the parameters that affect the problem, such as the length of the beam, the types of damage induced by real earthquake loading, etc.

8. Conclusions

This paper is focused on the calculation of the rotational capacity of steel beams at elevated temperatures. Moreover, a failure criterion for the determination of the fire-resistance of steel frame-structures under fire and FAE loading is proposed. To this end, three-dimensional shell finite element models are used for the simulation of the behaviour of I-beams at elevated temperatures. First, the models are validated against published experimental results. The evaluation of the rotational capacity of the pre-damaged beam at elevated temperatures is based on the standard beam approach. Cyclic loading is used in order to simulate the damage that is induced at the ends of the beams, that is actually a member of frame structure, due to earthquake loading. Different cyclic loading patterns are introduced in order to induce a specified "level of damage" in the beam. The ductility of the beams is obtained through virtual three-point bending tests (monotonic loading), which follow the cyclic loading stage. Parametric analyses are conducted with respect to the amplitude of the initial imperfections and to the different amplitudes of the cyclic loading pattern, at elevated temperatures. The failure criterion that is proposed in this paper is the value of the rotation that corresponds to the exhaustion of the available rotational capacity of the beam. The term *ultimate available rotation* is used to identify this rotation. It is concluded that, clearly, the ultimate available rotation depends on the amplitude of the initial imperfections and on the "level of damage" induced due to the cyclic loading.

Acknowledgments

This research has been co-financed by the European

Union (European Social Fund – ESF) and Greek national funds through the Operational Program "Education and Lifelong Learning" of the National Strategic Reference Framework (NSRF) - Research Funding Program: Heracleitus II. Investing in knowledge society through the European Social Fund.

References

Della Corte, G., Landolfo, R. and Mazzolani, F.M. (2003), "Post-earthquake fire resistance of moment resisting steel frames", *Fire Safety J.*, **38**(7), 593-612.

Dharma, R. and Tan, K.H. (2007a), "Rotational capacity of steel I-beams under fire conditions Part I: Experimental study", *Eng. Struct.*, **29**(9), 2391-2402.

Dharma, R. and Tan, K.H. (2007b), "Rotational capacity of steel I-beams under fire conditions Part II: Numerical simulations", *Eng. Struct.*, **29**(9), 2403-2418.

Eurocode 8 (2004), Design of Structures for Earthquake Resistance – Part 1: General rules seismic actions and rules for buildings, Brussels, Belgium.

Eurocode 3 (2003), Design of Steel Structures – Part 1-2: General Rules – Structural fire design, Brussels, Belgium.

Faggiano, B. and Mazzolani, F.M. (2011), "Fire after earthquake robustness evaluation and design: Application to steel structures", *Steel Constr. Des. Res.*, **4**(3), 183-187.

Faggiano, B., Espoto, M., Mazzolani, F.M. and Landolfo, R. (2007), "Fire analysis of steel portal frames damaged after earthquake according to performance based design", Urban Habitat Constructions under Catastrophic Events, Cost C26, Workshop, Prague, Czech Republic.

Faggiano, B., Espoto, M., Zaharia, R. and Pintea, D. (2008), "Structural analysis in case of fire after earthquake", Urban Habitat Constructions under Catastrophic Events, Cost Action C26, Malta University, Malta.

Franssen, J.M. and Vila Real, P. (2010), *Fire Design of Steel Structures, ECCS Eurocode Design Manuals*, (1st Ed.), Ernst & Sohn – A Wiley Company.

Gioncu, V. and Mazzolani, F. (2002), *Ductility of Seismic Resistant Steel Structures*, Spon Press, New York, NY, USA.

Gioncu, V. and Petcu, D. (2007), "Available rotational capacity of wide flange beams and beam-columns Part 1. Theoretical approaches", *J. Constr. Steel Res.*, **43**(1), 161-217.

Keller, W. (2012), "Thermomechanical response of steel moment-frame beam-column connections during post-earthquake Fire Exposure", Ph.D. Dissertation; Lehigh University, Bethlehem, PA, USA.

Keller, W. and Pessiki, S. (2012), "Effect of earthquake-induced damage to spray-applied fire-resistive insulation on the response of steel moment-frame beam-column connections during fire exposure", *J. Fire Prot. Eng.*, **22**(4), 271-299.

Kodur, V. and Dwaikat, M. (2009), "Response of steel beam-columns exposed to fire", *Eng. Struct.*, **31**(2), 369-379.

Lee, S., Davidson, R., Ohnishi, N. and Scawthorn, C. (2008), "Fire following earthquake — Reviewing the state-of-the-art of modeling", *Earthq. Spectra*, **24**(4), 933-967.

MSC Software Corporation (2010), MSC Marc Volume A: Theory and User Information, USA.

Poh, K.W. (2001), "Stress-strain temperature relationship for structural steel", *J. Mater. Civil Eng.*, **13**(5), 371-379.

Scawthorn, C., Eidinger, J.M. and Schiff, A. (2005), "Fire following earthquake", Technical Council on Lifeline Earthquake Engineering Monograph 26: 345, American Society of Civil Engineers, Reston, VA, USA.

Yassin, H., Iqbal, F., Bagchi, A. and Kodur, V.K.R. (2008), "Assessment of post-earthquake fire performance of steel-frame buildings", *Proceedings of 14th World Conference on Earthquake Engineering*, Beijing, China, October.

Zaharia, R. and Pintea, D. (2009), "Fire after earthquake analysis of steel moment resisting frames", *Int. J. Steel Struct.*, **9**(4), 275-284.

Zaharia, R., Pintea, D. and Dubina, D. (2008) "Fire after earthquake- a natural fire approach", *Proceedings of the 5th International Conference EUROSTEEL*, Graz, Austria, September.

Zaharia, R., Pintea, D. and Dubina, D. (2009), "Fire analysis of structures in seismic areas", *Proceedings of the International Conference on Application of Structural Fire Engineering*, Prague, Czech Republic.

Zhao, S. (2010), "GisFFE—an integrated software system for the dynamic simulation of fires following an earthquake based on GIS", *Fire Safety J.*, **45**(2), 83-97.

CC